Clean Energy Science and Technology 2025, 3(1), 286.
https://doi.org/10.18686/cest286

Article

Possibility of the application of Si_5O_{10}–Ge_5O_{10} for increasing H-adsorption towards the energy storage in transistors rather than Li-ion batteries

Fatemeh Mollaamin

Department of Biomedical Engineering, Faculty of Engineering and Architecture, Kastamonu University, Kastamonu 37150, Turkey;
fmollaamin@kastamonu.edu.tr

CITATION

Mollaamin F. Possibility of the application of Si_5O_{10}–Ge_5O_{10} for increasing H-adsorption towards the energy storage in transistors rather than Li-ion batteries. Clean Energy Science and Technology. 2025; 3(1): 286.
https://doi.org/10.18686/cest286

ARTICLE INFO

Received: 6 December 2024
Accepted: 8 January 2025
Available online: 5 February 2025

Abstract: A comprehensive investigation on hydrogen grabbing via Si_5O_{10}–Ge_5O_{10} was carried out including using density functional theory computations. The data showed that when silicon was replaced with germanium, the hydrogen-grabbing energy was ameliorated. The electromagnetic and thermodynamic properties of Si_5O_{10}–Ge_5O_{10} and $Li_2(Si_5O_{10}$–$Ge_5O_{10})$ nanoclusters were evaluated. The fluctuation in charge density values demonstrated that electronic densities were mainly located in the boundary of adsorbate/adsorbent atoms during adsorption. Therefore, it can be concluded that the Si_5O_{10}–Ge_5O_{10} nanocluster might be an appropriate candidate for hydrogen storage in transistors. Lithium has an advantage over Si/Ge for possessing higher electron-and-hole motion, which allows lithium instruments to operate at higher frequencies than Si/Ge instruments.

Keywords: lithium battery; $Li_2(Si_5O_{10}$–$Ge_5O_{10})$; Si_5O_{10}–Ge_5O_{10}; hydrogen storage; DFT

1. Introduction

A fuel cell applies reverse electrolysis to convert an oxidizing agent and hydrogen to power an electric motor [1–4]. Carbon nanotubes (CNTs), owing to their lightness, tube construction, vast plane and high reactivity between C and H atoms, can be proposed as a promising material for hydrogen grabbing (H-grabbing) [5–8].

It has been investigated that hydrogen storing in C-nanocompounds indicates molecular hydrogen dissociation [9–12]. The structure of transition metal–carbon bonding exhibits a charge distribution among the boundary atoms, and the cationic state of transition metals has been discussed [13–17]. Thus, an electronic charge can be produced through gas-molecule adsorption on the surface of an ionic transition metal [18–20]. Transition metals as dopants might make a whole Hamiltonian perturbation towards alterations in electronic structures, which has substantial use in magnetic electronic instruments [21–25]. Recently, Si-, Ge- or Sn-carbide nanostructures have been suggested as engaged H-grabbing compounds [26–28]. Since the polarizability of silicon is higher than that of carbon, it is supposed that Si–C/Si nanosheets might attach to compositions more strongly in comparison with net carbon nano-surfaces [29–31].

Moreover, the adsorption and sensing of H_2 and CH_2O molecules on pristine and transition metals consist of V, Cr, Mn, Nb, Mo, Tc, Ta, W or Re doping on B or N sites of boron nitride nanosheets (BNNSs). The achieved results exhibit that pristine BNNS indicates a fragile interaction with H_2 and CH_2O molecules. The H_2 and CH_2O molecules might be strongly adsorption on the transition-metal-doped BNNSs with appreciable adsorption energy through the geometrical deformation on the transition metal doping zone [32].

In the author's previous works, the investigation of energy storage in fuel cells through hydrogen adsorption has been accomplished using density functional theory (DFT) calculations through different nanomaterials consisting of silicon/germanium/tin/lead nano-carbides [33], magnesium-aluminum alloy [34] and aluminum/carbon/ silicon doping boron nitride nanocage [35–39].

Nanomaterials with remarkable specific structures indicate promising applications in the field of energy storage, electrocatalysis and fuel cells. This article sought to demonstrate a facile approach for fabricating the nanoclusters of Si_5O_{10}–Ge_5O_{10} as a template under a moderate condition for hydrogen storage [40–42].

The present research aimed to explore the possibility of using Si_5O_{10}–Ge_5O_{10} nanoclusters for hydrogen storage by employing first-principles calculations. We analyzed the structural and electronic properties of Si_5O_{10}, Ge_5O_{10}, Si_5O_{10}–Ge_5O_{10}, $Li_2(Si_5O_{10}$–$Ge_5O_{10})$ and the hydrated nanoclusters of $H_2(Si_5O_{10}$–$Ge_5O_{10})$ and $Li_2H_4(Si_5O_{10}$–$Ge_5O_{10})$ using state-of-the-art computational techniques.

2. Materials modeling by novel compounds

The hydrated nanoclusters of $H_2(Si_5O_{10}$–$Ge_5O_{10})$ and $Li_2H_4(Si_5O_{10}$–$Ge_5O_{10})$ were modeled in the presence of Si_5O_{10} and Ge_5O_{10} and the production of Si_5O_{10}–Ge_5O_{10} and $Li_2(Si_5O_{10}$–$Ge_5O_{10})$, which can increase hydrogen storage in semiconductor transistors. In this research, calculations were done by using the CAM–B3LYP–D3 /EPR–3 level of theory (**Figure 1**). In addition, a new hybrid exchange-correlation functional called CAM–B3LYP was suggested, which merges B3LYP and long-range correction [43]. Moreover, DFT functionals with Grimme's D3 correction were considered [44]. The approach of dispersion correction was added to the Kohn-Sham density functional theory (DFT-D) with higher accuracy [45].

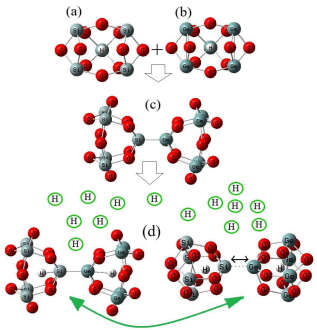

Figure 1. Formation of **(a)** Si_5O_{10} and **(b)** Ge_5O_{10} into **(c)** Si_5O_{10}–Ge_5O_{10} towards formation of **(d)** $H_2(Si_5O_{10}$–$Ge_5O_{10})$ to increase hydrogen adsorption for saving energy in transistors.

Figure 1 shows the process of hydrogen adsorption on the surface of Si_5O_{10}–Ge_5O_{10}, which includes the formation of hydrated nanoclusters containing H–Si_5O_{10}, H–Ge_5O_{10} and H–Si_5O_{10}–Ge_5O_{10}–H. The Bader charge analysis [46] was utilized to examine the trapping of hydrogen atoms by Si_5O_{10}–Ge_5O_{10} and the formation of HSi_5O_{10}, HGe_5O_{10}, $H_2(Si_5O_{10}$–$Ge_5O_{10})$ and $Li_2H_4(Si_5O_{10}$–$Ge_5O_{10})$ nanoclusters (**Figure 1**). The analysis of the rigid potential energy surface using the DFT [47–49] was performed using the Gaussian 16 (revision C.01) program package [50] and

GaussView 6.1 [51]. The coordination input for H-grabbing by Si_5O_{10}–Ge_5O_{10} and $Li_2(Si_5O_{10}$–$Ge_5O_{10})$ was applied using 6-311+G (d, p) and EPR–3 basis sets.

3. Results and discussion

3.1. Density of states and partial density of states

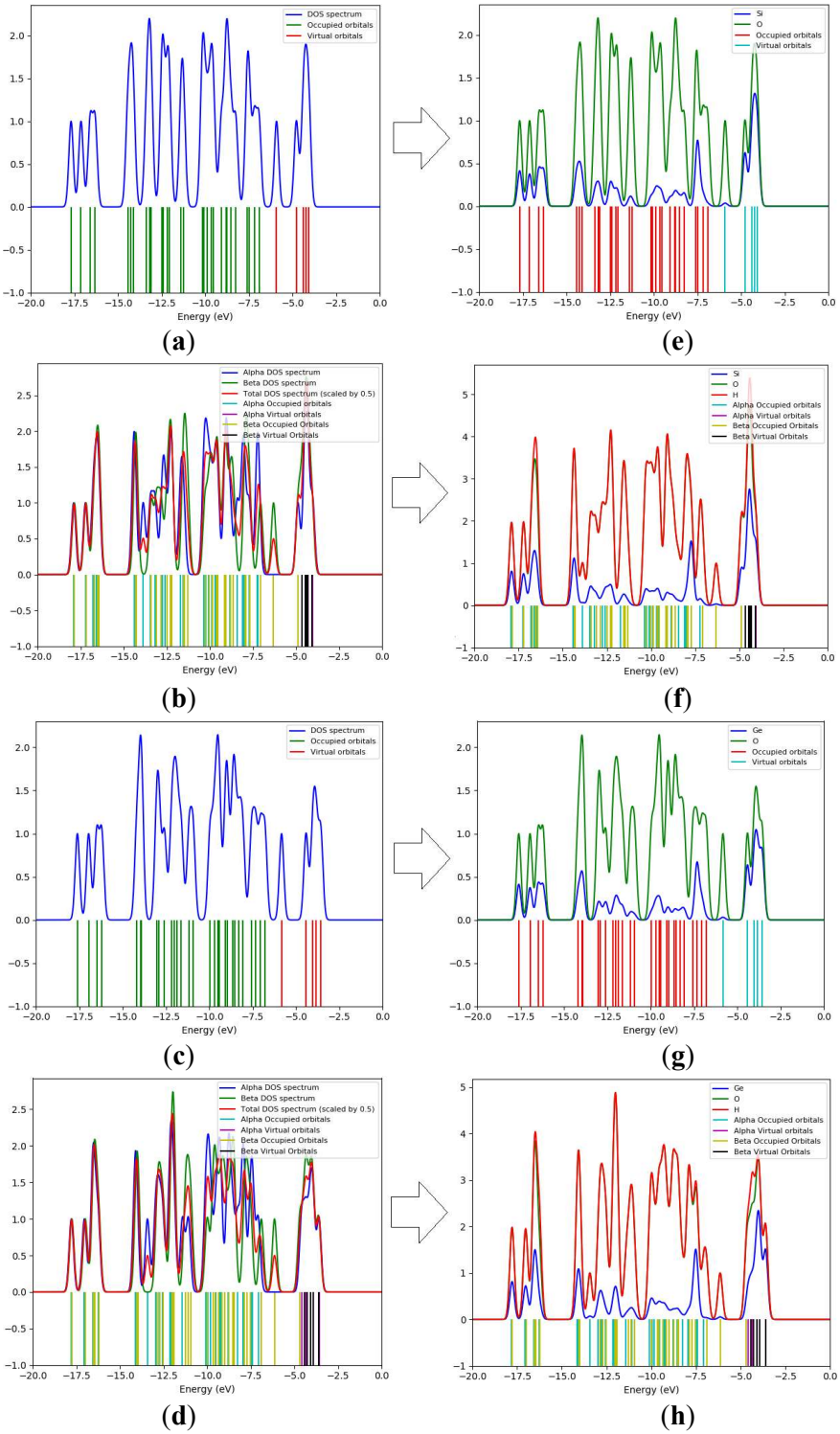

Figure 2. DOS of **(a)** Si_5O_{10}, **(b)** HSi_5O_{10}, **(c)** Ge_5O_{10} and **(d)** HGe_5O_{10} nanoclusters. PDOS of **(e)** Si_5O_{10}, **(f)** HSi_5O_{10}, **(g)** Ge_5O_{10} and **(h)** HGe_5O_{10} nanoclusters.

The electronic structures of hydrogen adsorption by Si_5O_{10} and Ge_5O_{10} as the selective sensor for detecting and grabbing hydrogen atoms were investigated to simplify the subsequent study for interfacial electronic properties using the CAM–B3LYP–D3/6-311+G (d, p)//LANL2DZ level of theory. **Figures 2a–2h** show the density of states (DOS) and partial density of states (PDOS) of Si_5O_{10}, HSi_5O_{10}, Ge_5O_{10} and HGe_5O_{10}. The appearance of the energy states (*p*-orbital) of O, Si and Ge within the gap of Si_5O_{10} and Ge_5O_{10} induced the reactivity of the system. It is clear from the figures that after the grabbing of hydrogen atoms, there was a significant contribution by *p*-orbitals in the unoccupied level for grabbing hydrogen atoms. Therefore, the DOS and PDOS values showed that the *p* states of the O, Si and Ge atoms were overcome due to the conduction band.

Figures 2a and **2e** show that Si_5O_{10} has sharp peaks for O around –7.5 and –12.5 eV, while HSi_5O_{10} (**Figures 2b** and **2f**) exhibited sharp peaks around –5 eV for H atoms. Furthermore, Ge_5O_{10} exhibited sharp peaks for O around –7.5 and –12.5 eV (**Figures 2c** and **2g**). However, HGe_5O_{10} exhibited sharp peaks around –12.5 eV for H atoms (**Figures 2d** and **2h**).

The resulting DOS and PDOS could also be used to estimate the charge assembly between Si_5O_{10} and Ge_5O_{10} through hydrogen adsorption. In addition, the results illustrated that the dominant complexes of the metalloid/semiconductor attribute of silicon and germanium accompanying an exact degree of covalent traits could describe the augmenting of the stability of Si_5O_{10}–Ge_5O_{10} during the process of H-adsorption.

3.2. Theory of nuclear quadrupole resonance (NQR)

NQR frequencies were measured for Si_5O_{10}, HSi_5O_{10}, Ge_5O_{10} and HGe_5O_{10} for estimating the hydrated nanoclusters of $H_2(Si_5O_{10}$–$Ge_5O_{10})$ (**Table 1**). The NQR method is related to the multipole expansion in Cartesian coordinates, as in Equation (1) [52,53]:

$$V(r) = V(0) + \left[\left(\frac{\partial V}{\partial x_i}\right)\Big|_0 . x_i\right] + \frac{1}{2}\left[\left(\frac{\partial^2 V}{\partial x_i x_j}\right)\Big|_0 . x_i x_j\right] + \cdots \quad (1)$$

After simplification, there are only second derivatives related to the identical variable for potential energy [52–55]:

$$U = -\frac{1}{2}\int_{\mathcal{D}} d^3 r \rho_r \left[\left(\frac{\partial^2 V}{\partial x_i^2}\right)\Big|_0 . x_i^2\right] = -\frac{1}{2}\int_{\mathcal{D}} d^3 r \rho_r \left[\left(\frac{\partial E_i}{\partial x_i}\right)\Big|_0 . x_i^2\right] = -\frac{1}{2}\left(\frac{\partial E_i}{\partial x_i}\right)\Big|_0 . \int_{\mathcal{D}} d^3 r [\rho(r) . x_i^2] \quad (2)$$

The "electric potential" through carrying over the electric charge was measured for Si_5O_{10}, HSi_5O_{10}, Ge_5O_{10} and HGe_5O_{10} complexes (**Table 1**).

Table 1. Electric potential (E_p, in unit of a.u.) and Bader charge (Q, in unit of coulomb) through NQR calculation for Si_5O_{10}, HSi_5O_{10}, Ge_5O_{10} and HGe_5O_{10} complexes.

Si_5O_{10}			**HSi_5O_{10}**		
Atom	***Q***	***E_p***	**Atom**	***Q***	***E_p***
Si1	1.4239	−49.0914	Si1	1.4421	−49.0827
O2	−0.6277	−22.2955	O2	−0.618	−22.2979
O3	−0.7947	−22.3347	O3	−0.7537	−22.3135
Si4	1.4234	−49.0924	Si4	1.4362	−49.0907

Table 1. (*Continued*).

Si_5O_{10}			**HSi_5O_{10}**		
Atom	***Q***	***E_p***	**Atom**	***Q***	***E_p***
Si5	1.4216	−49.0941	Si5	1.4469	−49.0917
Si6	1.4226	−49.0928	Si6	1.4338	−49.083
O7	−0.6507	−22.3028	O7	−0.6858	−22.3341
O8	−0.7940	−22.3344	O8	−0.7431	−22.3061
O9	−0.7379	−22.3157	O9	−0.7427	−22.3249
O10	−0.7654	−22.3384	O10	−0.7432	−22.3262
O11	−0.7589	−22.3475	O11	−0.7355	−22.3386
O12	−0.7460	−22.3127	O12	−0.7283	−22.3219
Si13	1.4556	−49.0976	Si13	1.4714	−49.0849
O14	−0.6430	−22.2988	O14	−0.6439	−22.3063
O15	−0.6285	−22.2976	O15	−0.6788	−22.3423
			H16	−0.1566	−0.77032
Ge_5O_{10}			**HGe_5O_{10}**		
Atom	***Q***	***E_p***	**Atom**	***Q***	***E_p***
Ge1	1.4949	−155.046	Ge1	1.5230	−155.039
O2	−0.6640	−22.3144	O2	−0.6530	−22.3216
O3	−0.8300	−22.3494	O3	−0.7816	−22.3284
Ge4	1.4995	−155.048	Ge4	1.5166	−155.044
Ge5	1.4907	−155.049	Ge5	1.5213	−155.044
Ge6	1.4963	−155.048	Ge6	1.5167	−155.039
O7	−0.6867	−22.3203	O7	−0.7206	−22.3472
O8	−0.8299	−22.3506	O8	−0.7691	−22.3215
O9	−0.7767	−22.3343	O9	−0.7851	−22.3477
O10	−0.8072	−22.3585	O10	−0.7854	−22.3492
O11	−0.8007	−22.3677	O11	−0.7801	−22.3583
O12	−0.7853	−22.3343	O12	−0.7653	−22.3421
Ge13	1.5320	−155.055	Ge13	1.5653	−155.044
O14	−0.6736	−22.3169	O14	−0.7009	−22.3379
O15	−0.6591	−22.3163	O15	−0.6961	−22.3488
			H16	−0.2056	−0.78454

The Si, Ge, O and hydrogen atoms absorbed on Si_5O_{10} and Ge_5O_{10} were calculated through Q and E_p properties. The values show that by augmenting the negative charge of various atoms, the electric potential extracted from NQR calculations increased. In addition, the elements of O2, O3, O7, O8, O9, O10, O11, O12, O14 and O15 of Si_5O_{10} and Ge_5O_{10} exhibited the most efficiency for admitting electrons from the electron donor of H16 adsorbed on Si_5O_{10} and Ge_5O_{10} (**Table 1** and **Figure 3**).

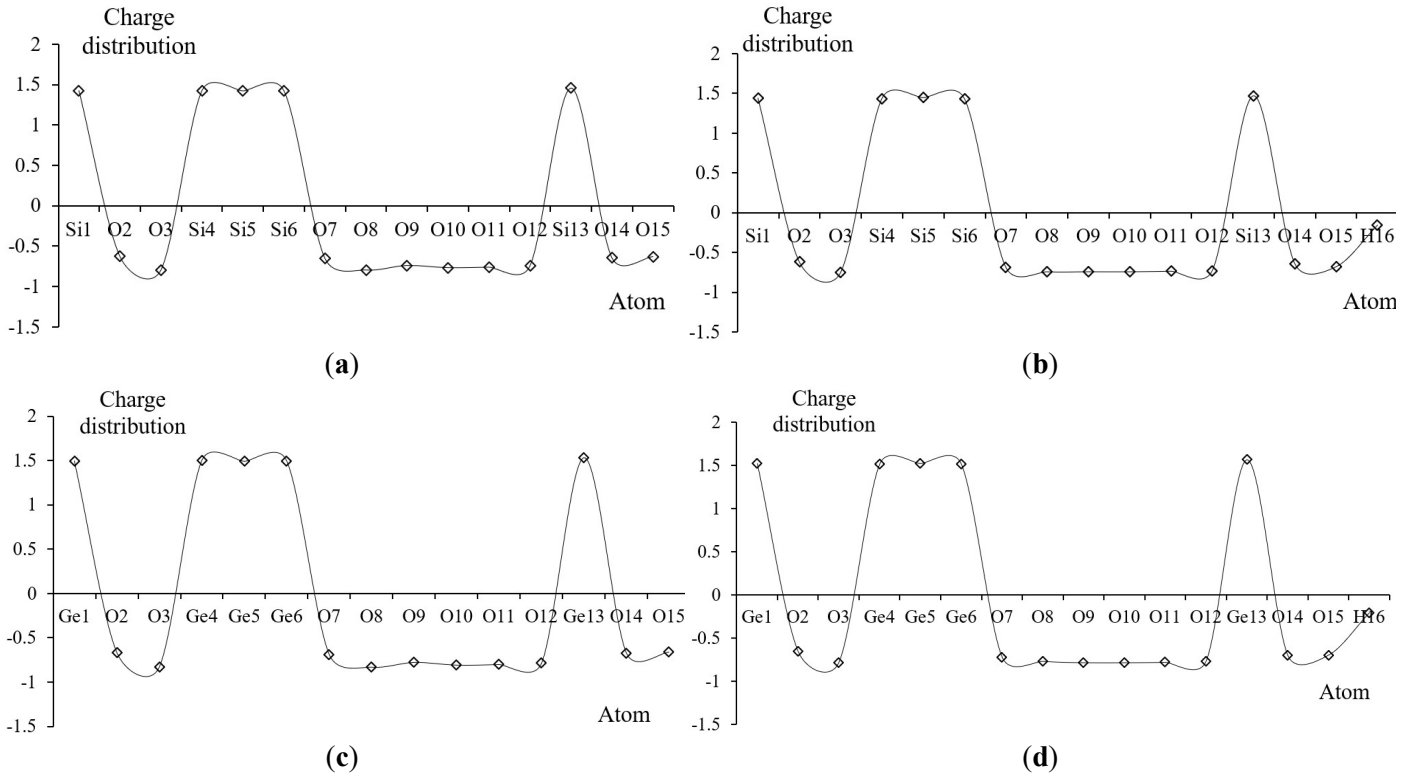

Figure 3. Charge distribution (Q) of active atoms in **(a)** Si_5O_{10}, **(b)** HSi_5O_{10}, **(c)** Ge_5O_{10} and **(d)** HGe_5O_{10} nanoclusters.

Figures 4a–4d show E_p versus Q for Si, Ge, O and hydrogen atoms absorbed on Si_5O_{10} and Ge_5O_{10}.

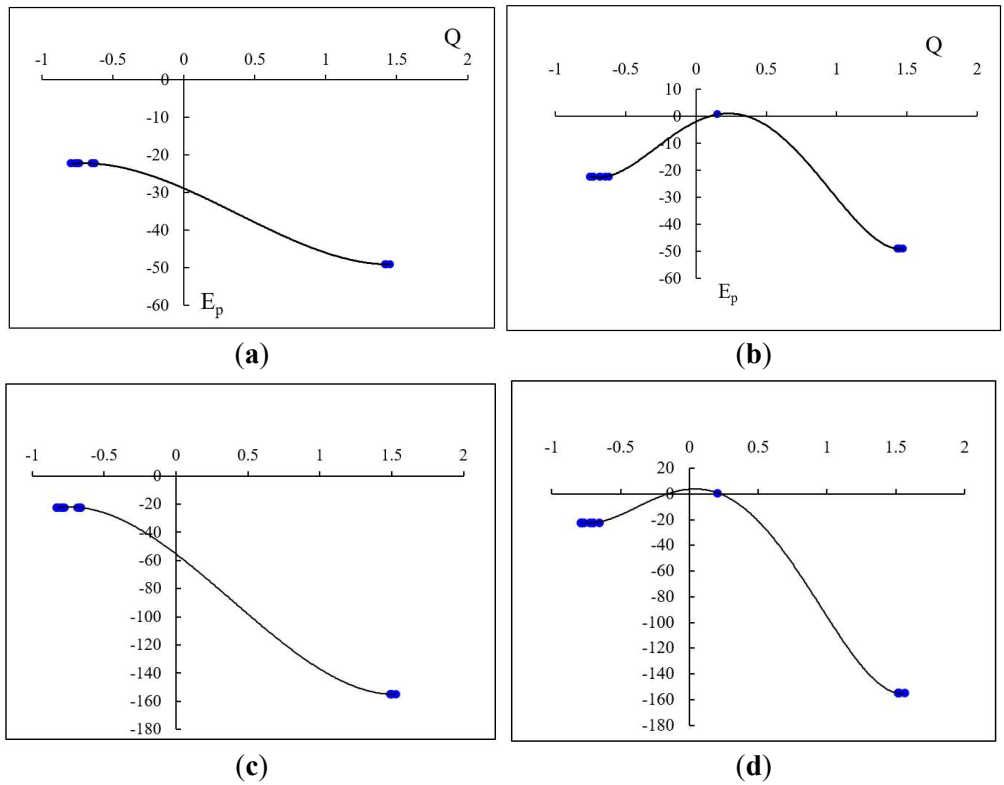

Figure 4. E_p versus Q from NQR calculations for **(a)** Si_5O_{10}, **(b)** HSi_5O_{10}, **(c)** Ge_5O_{10} and **(d)** HGe_5O_{10} nanoclusters.

In **Figure 4a**, it was observed that the behavior of Si and O atoms in Si_5O_{10} showed high sensitivity, based on the correlation coefficient of $R^2 = 0.9999$. **Figure 4b** shows that hydrogen adsorption on Si_5O_{10} (HSi_5O_{10}) showed high sensitivity, with $R^2 = 0.9999$. In **Figure 4c**, it was observed that the behavior of Ge and O atoms in Ge_5O_{10}, as well as hydrogen adsorption on Ge_5O_{10} (HGe_5O_{10}) (**Figure 4d**), showed high sensitivity, with $R^2 = 1$. The fluctuated peaks for E_p have been shown to be around the values of hydrogen adsorption on Si_5O_{10} and Ge_5O_{10}, which demonstrated the electron-acceptance of hydrogen versus those of Si, Ge and O atoms of Si_5O_{10} and Ge_5O_{10} (**Figures 2a** and **2d**). Based on the results, there can be renewed interest in the combination of silicon and germanium as the Si_5O_{10}–Ge_5O_{10} nanocluster for potential applications in next-generation electronics.

3.3. Analysis of nuclear magnetic resonance (NMR) spectra

NMR spectra of Si_5O_{10} and Ge_5O_{10} complexes as potential molecules for hydrogen storage can unravel the efficiency of these complexes in saving energy. DFT calculations were performed to attain the chemical shielding tensors in the principal axes system to estimate the values of isotropic chemical shielding (σ_{iso}) and anisotropic chemical shielding (σ_{aniso}) [56,57] (**Table 2**):

$$\sigma_{\text{iso}} = (\sigma_{11} + \sigma_{22} + \sigma_{33})/3 \quad (3)$$

$$\sigma_{\text{aniso}} = \sigma_{33} - (\sigma_{22} + \sigma_{11})/2 \quad (4)$$

Table 2. Magnetic resonance (ppm) for selected atoms of Si_5O_{10}, HSi_5O_{10}, Ge_5O_{10} and HGe_5O_{10}.

Si_5O_{10}			**HSi_5O_{10}**		
Atom	**σ_{iso}**	**σ_{aniso}**	**Atom**	**σ_{iso}**	**σ_{aniso}**
Si1	554.0642	419.0832	Si1	636.0795	83.3146
O2	48.4001	1103.1680	O2	197.7138	180.5182
O3	719.1992	1393.8472	O3	213.8981	571.6387
Si4	606.8573	283.5283	Si4	612.4946	136.0914
Si5	515.0784	300.3033	Si5	590.5624	112.0924
Si6	499.4416	298.5084	Si6	640.6146	109.0061
O7	165.2869	1989.8484	O7	257.4682	540.4664
O8	446.3837	1626.0109	O8	345.3073	760.8007
O9	644.0032	1145.0143	O9	396.4206	516.7599
O10	258.2121	801.0630	O10	291.9858	500.1157
O11	59.3078	646.4488	O11	381.7876	579.4428
O12	777.7640	1673.7326	O12	592.8797	761.1373
Si13	676.7427	69.9662	Si13	700.3543	80.4624
O14	644.6460	1598.2955	O14	192.6514	365.7050
O15	640.6636	1233.6320	O15	575.7311	737.1360
			H16	33.8812	5.1474
Ge_5O_{10}			**HGe_5O_{10}**		
Atom	**σ_{iso}**	**σ_{aniso}**	**Atom**	**σ_{iso}**	**σ_{aniso}**
Ge1	11774.5678	78310.4000	Ge1	2269.9670	265.4637

Table 2. (*Continued*).

Ge_5O_{10}			HGe_5O_{10}		
Atom	σ_{iso}	σ_{aniso}	**Atom**	σ_{iso}	σ_{aniso}
O2	7981.0314	45129.9129	O2	185.7769	323.7807
O3	26849.6035	102235.8861	O3	234.9996	690.9768
Ge4	2860.0389	56431.2360	Ge4	2254.9254	354.3985
Ge5	22560.3347	50034.9570	Ge5	2196.2345	239.0115
Ge6	25249.1878	67283.2726	Ge6	2283.0559	294.6875
O7	28391.8831	116633.3581	O7	192.2913	265.9975
O8	19250.3259	151688.3405	O8	400.6946	945.3551
O9	8016.6504	16619.9360	O9	429.4418	692.5679
O10	12714.2137	20281.5576	O10	322.2798	641.0732
O11	9151.5705	14760.9081	O11	363.3794	661.7813
O12	45077.0106	82973.3504	O12	644.3035	1039.2395
Ge13	1836.0321	6719.1076	Ge13	2377.4219	144.0036
O14	21908.3686	61863.1557	O14	93.6525	302.7204
O15	6288.9475	33932.6037	O15	457.9994	712.9732
			H16	38.0125	2.7857

In **Table 2**, the NMR data showed remarkable values for hydrogen atoms, which were adsorbed on Si_5O_{10} and Ge_5O_{10} complexes. The observed increase in the chemical shift anisotropy spans for H-atom adsorption on Si_5O_{10} and Ge_5O_{10} complexes are near O2, O3, O7, O8, O12, O14 and O15. The notable fragile signal intensity close to the parallel edge of the nanocluster sample might be owing to the non-spherical distribution of these clusters as induced by silicon or germanium binding (**Figures 5a–5d**).

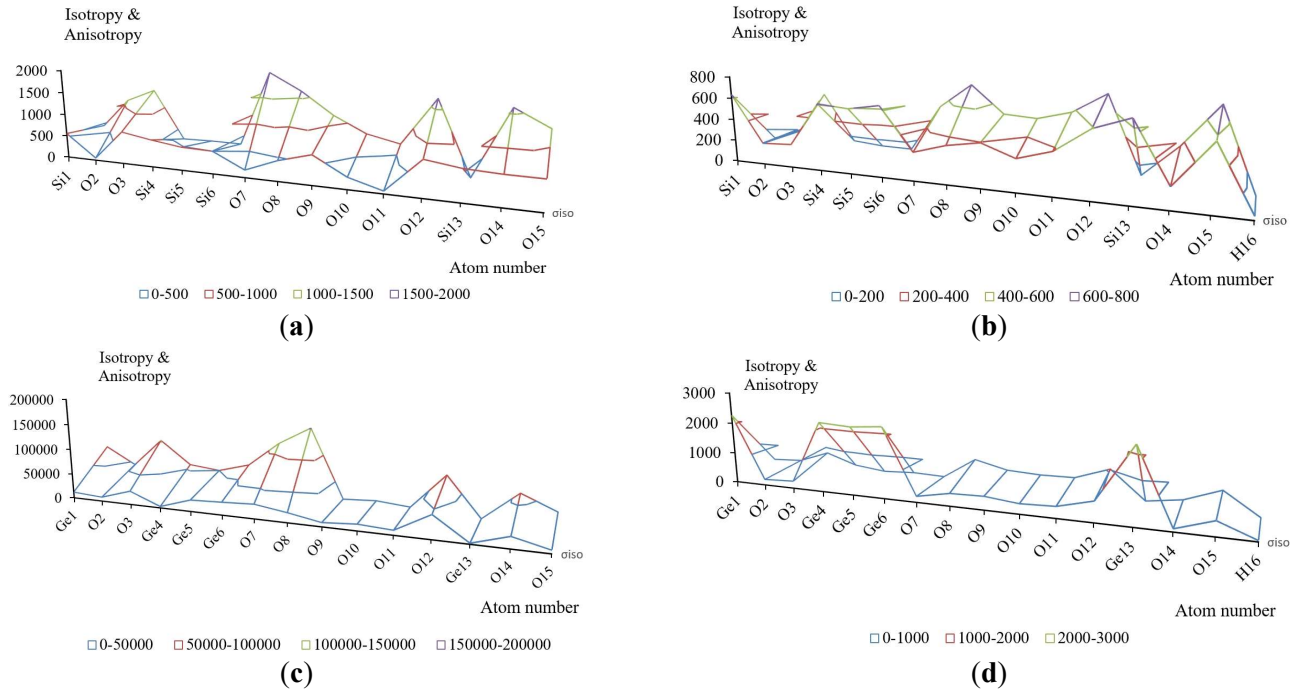

Figure 5. NMR spectra for **(a)** Si_5O_{10}, **(b)** HSi_5O_{10}, **(c)** Ge_5O_{10} and **(d)** HGe_5O_{10} complexes.

The NMR spectroscopy results showed the chemical shielding between silicon and oxygen in Si_5O_{10} (**Figure 5a**); between hydrogen, silicon and oxygen in HSi_5O_{10} (**Figure 5b**); between germanium and oxygen in Ge_5O_{10} (**Figure 5c**) and between hydrogen, germanium and oxygen in HGe_5O_{10} (**Figure 5d**). The yield of electromagnetic shifting can be directed by oxygen atoms of O3, O7, O12 and O14 in Si_5O_{10} (**Figure 5a**); by O3, O8, O12 and O15 in HSi_5O_{10} (**Figure 5b**); by O3, O8, O12 and O14 in Ge_5O_{10} (**Figure 5c**) and by Ge1, Ge4, Ge5, Ge6 and Ge13 in HGe_5O_{10} (**Figure 5d**). The results showed that the intensity for hydrogen adsorption can be developed in Ge_5O_{10} through germanium atoms compared with silicon atoms in Si_5O_{10}. Although both silicon and germanium are semiconductor elements, germanium can be more conductive than silicon in transistors due to its high semiconducting properties. Therefore, based on the structural studies, it would be advantageous to model a novel Si_5O_{10}–Ge_5O_{10} complex for increasing the adsorption of hydrogen atoms in transistors.

3.4. Thermodynamic properties

From **Table 3**, it can be concluded through thermodynamic specifications that the $Li_2(Si_5O_{10}–Ge_5O_{10})$ nanocluster might be a more efficient structure for hydrogen trapping.

Table 3. Thermochemistry of (a) $Si_5O_{10}–Ge_5O_{10}$, (b) $H_2(Si_5O_{10}–Ge_5O_{10})$, (c) $Li_2(Si_5O_{10}–Ge_5O_{10})$ and (d) $Li_2H_4(Si_5O_{10}–Ge_5O_{10})$ nanoclusters.

Compound	$\Delta E^o_{ads} \times 10^{-3}$	$E_{H-b} \times 10^{-3}$	$\Delta H^o_{ads} \times 10^{-3}$	$\Delta G^o_{ads} \times 10^{-3}$
Si_5O_{10}	−1379.647	−0.29	−1379.647	−1379.646
HSi_5O_{10}	−1379.937	-	−1379.936	−1379.965
Ge_5O_{10}	−6981.158	−0.286	−6981.158	−6981.189
HGe_5O_{10}	−6981.444	-	−6981.443	−6981.474
$Si_5O_{10}–Ge_5O_{10}$	−8360.864	−0.508	−8360.864	−8360.892
$H_2(Si_5O_{10}–Ge_5O_{10})$	−8361.372	-	−8361.371	−8361.390
$Li_2(Si_5O_{10}–Ge_5O_{10})$	−9176.639	−1.455	−9176.639	−9176.671
$Li_2\ H_4(Si_5O_{10}–Ge_5O_{10})$	−91,178.094	-	−9178.094	−9178.114

The thermodynamic parameters of hydrogen adsorption on $Si_5O_{10}–Ge_5O_{10}$ and $Li_2(Si_5O_{10}–Ge_5O_{10})$ nanoclusters were assigned through a given number of hydrogen donor sites. The stability of the linkage between the two complexes of Si_5O_{10} and Ge_5O_{10} and the formation of the $Si_5O_{10}–Ge_5O_{10}$ nanocluster can be considered as $Li_2H_4(Si_5O_{10}–Ge_5O_{10}) > H_2(Si_5O_{10}–Ge_5O_{10}) > HGe_5O_{10} > HSi_5O_{10}$ (**Table 3**).

The maximum efficiency of $Si_5O_{10}–Ge_5O_{10}$ for hydrogen adsorption through ΔG^o_{ads} is related to the linkage between hydrogen atoms with silicon and germanium in $Si_5O_{10}–Ge_5O_{10}$ and $Li_2(Si_5O_{10}–Ge_5O_{10})$ and the formation of hydrated nanoclusters of $H_2(Si_5O_{10}–Ge_5O_{10})$ and $Li_2H_4(Si_5O_{10}–Ge_5O_{10})$. The adsorption process of hydrogen atoms in Si_5O_{10}, Ge_5O_{10}, $Si_5O_{10}–Ge_5O_{10}$ and $Li_2(Si_5O_{10}–Ge_5O_{10})$ nanoclusters is affirmed by the ΔG^o_{ads} quantities:

$$\Delta G^o_{ads(1)} = \Delta G^o_{H_2[Si_5O_{10}-Ge_5O_{10}]} - \left(\Delta G^o_{Si_5O_{10}} + \Delta G^o_{HSi_5O_{10}} + \Delta G^o_{Ge_5O_{10}} + \Delta G^o_{HGe_5O_{10}}\right) \quad (5)$$

$$\Delta G^o_{ads(2)} = \Delta G^o_{Li_2H_4[Si_5O_{10}-Ge_5O_{10}]} - \left(\Delta G^o_{Li_2[Si_5O_{10}-Ge_5O_{10}]} + \Delta G^o_{Si_5O_{10}-Ge_5O_{10}}\right) \quad (6)$$

This shows the interaction between hydrogen atoms and Si_5O_{10}, Ge_5O_{10}, Si_5O_{10}–Ge_5O_{10} and $Li_2(Si_5O_{10}–Ge_5O_{10})$ nanoclusters as electron acceptors. Therefore, the combination of Si_5O_{10} and Ge_5O_{10} to produce the $Si_5O_{10}–Ge_5O_{10}$ nanocluster can enhance hydrogen storage in transistors through the formation of the hydrated cluster of $H_2(Si_5O_{10}–Ge_5O_{10})$.

4. Conclusion

In summary, H-grabbing in the nanoclusters of Si_5O_{10}, Ge_5O_{10} and $Si_5O_{10}–Ge_5O_{10}$ was investigated by using first-principles computations. The alterations of charge density illustrated a remarkable charge transfer towards Si_5O_{10}, Ge_5O_{10} and Si_5O_{10}–Ge_5O_{10}. The fluctuation in charge density values demonstrates that the electronic densities were in the boundary of adsorbate/adsorbent atoms during adsorption. Besides that, the thermodynamic parameters describing H-grabbing in the nano-carbides of Si_5O_{10}, Ge_5O_{10} and $Si_5O_{10}–Ge_5O_{10}$ were investigated, including the internal process of the adsorbent-adsorbate system. The combination of Si_5O_{10} and Ge_5O_{10} to produce the $Si_5O_{10}–Ge_5O_{10}$ nanocluster can enhance hydrogen storage in transistors through the formation of the hydrated clusters of $H_2(Si_5O_{10}–Ge_5O_{10})$. Moreover, hydrogen bond (H-bond)-accepting sites by $Li_2(Si_5O_{10}–Ge_5O_{10})$ can alleviate parasitic hydrogen evolution in aqueous electrolytes in lithium-ion batteries. Today, it is crucial to distinguish the potential of hydrogen technologies and bring up all perspectives of their performance, from technological progress to economic and social effects. Authors should pursue research on sustainability and clean energy subjects towards finding new solutions for reducing the global dependency on fossil fuels.

Acknowledgments: In successfully completing this paper and its research, the author is grateful to Kastamonu University.

Conflict of interest: The author declares no conflict of interest.

References

1. Olabi AG, Sayed ET. Developments in Hydrogen Fuel Cells. Energies. 2023; 16(5): 2431. doi: 10.3390/en16052431
2. Feng X, Sun L, Wang W, et al. Construction of CdS@ZnO core–shell nanorod arrays by atomic layer deposition for efficient photoelectrochemical H_2 evolution. Separation and Purification Technology. 2023; 324: 124520. doi: 10.1016/j.seppur.2023.124520
3. Mollaamin F, Monajjemi M. In Silico-DFT Investigation of Nanocluster Alloys of Al-(Mg, Ge, Sn) Coated by Nitrogen Heterocyclic Carbenes as Corrosion Inhibitors. Journal of Cluster Science. 2023; 34: 2901-2918. doi: 10.1007/s10876-023-02436-5
4. Das V, Padmanaban S, Venkitusamy K, et al. Recent advances and challenges of fuel cell based power system architectures and control–A review. Renewable and Sustainable Energy Reviews. 2017; 73: 10-18. doi: 10.1016/j.rser.2017.01.148
5. Lobo R, Ribeiro J, Inok F. Hydrogen Uptake and Release in Carbon Nanotube Electrocatalysts. Nanomaterials. 2021; 11(4): 975. doi: 10.3390/nano11040975
6. Wang Z, Li J, Hu C, et al. Hybrid energy storage system and management strategy for motor drive with high torque overload. Journal of Energy Storage. 2024; 75: 109432. doi: 10.1016/j.est.2023.109432
7. Strobel R, Garche J, Moseley PT, et al. Hydrogen Storage by Carbon Materials. Journal of Power Sources. 2006; 159(2): 781-801. doi: 10.1016/j.jpowsour.2006.03.04
8. Baughman RH, Zakhidov AA, De Heer WA. Carbon Nanotubes–The Route toward Applications. Science. 2002; 297(5582): 787-792. doi: 10.1126/science.1060928

9. Fomkin A, Pribylov A, Men'shchikov I, et al. Adsorption-Based Hydrogen Storage in Activated Carbons and Model Carbon Structures. Reactions. 2021; 2(3): 209-226. doi: 10.3390/reactions2030014
10. Zhao Y, Kim YH, Dillon AC, et al. Hydrogen Storage in Novel Organometallic Buckyballs. Physical Review Letters. 2005; 95: 155504. doi: 10.1103/PhysRevLett.94.155504
11. Yang FH, Lachawiec AJ, Yang RT. Adsorption of Spillover Hydrogen Atoms on Single-Wall Carbon Nanotubes. The Journal of Physical Chemistry B. 2006; 110: 6236-6244. doi: 10.1021/jp056461u
12. Novoselov KS, Geim AK, Morozov SV, et al. Electric field effect in atomically thin carbon films. Science. 2004; 306: 666-669. doi: 10.1126/science.1102896
13. Mollaamin F, Shahriari S, Monajjemi M, et al. Nanocluster of Aluminum Lattice via Organic Inhibitors Coating: A Study of Freundlich Adsorption. Journal of Cluster Science. 2023; 34: 1547-1562. doi: 10.1007/s10876-022-02335-1
14. Castro Neto AH, Guinea F, Peres NMR, et al. The electronic properties of graphene. Review of Modern Physics. 2009; 81: 109-162. doi: 10.1103/RevModPhys.81.109
15. Mak KF, Lee C, Hone J, et al. Atomically thin MoS_2: A new direct-gap semiconductor. Physical Review Letters. 2010; 105: 136805-136807. doi: 10.1103/PhysRevLett.105.136805
16. Zan L, Amin HMA, Mostafa E, et al. Electrodeposited cobalt nanosheets on smooth silver as a bifunctional catalyst for OER and ORR: In situ structural and catalytic characterization. ACS Applied Materials & Interfaces. 2022; 14: 55458-55470. doi: 10.1021/acsami.2c12163
17. Zhao J, Kou M, Yuan Q, et al. Encapsulating Transition Metal Nanoparticles inside Carbon (TM@C) Chainmail Catalysts for Hydrogen Evolution Reactions: A Review. Molecules. 2024; 29: 4677. doi: 10.3390/molecules29194677
18. Low T, Rodin AS, Carvalho A, et al. Tunable optical properties of multilayer black phosphorus thin films. Physical Review B. 2014; 90: 075434-074538. doi: 10.1103/PhysRevB.90.075434
19. Fei R, Faghaninia A, Soklaski R, et al. Enhanced thermoelectric efficiency via orthogonal electrical and thermal conductances in phosphorene. Nano Letters. 2014; 14(11): 6393-6399. doi: 10.1021/nl502865s
20. Ramasubramaniam A, Muniz AR. Ab initio studies of thermodynamic and electronic properties of phosphorene nanoribbons. Physical Review B. 2014; 90: 085424-085429. doi: 10.1103/PhysRevB.90.085424
21. Yan Z, Bai Y, Sun L. Adsorption of thiophene and SO_x molecules on Cr-doped and Ti-doped graphene nanosheets: A DFT study. Materials Research Express. 2019; 6(12): 125067. doi: 10.1088/2053-1591/ab599d
22. Mollaamin F, Monajjemi M. In Situ Ti-Embedded SiC as Chemiresistive Nanosensor for Safety Monitoring of CO, CO_2, NO, NO_2: Molecular Modelling by Conceptual Density Functional Theory. Russian Journal of Physical Chemistry B. 2024; 18: 49-66. doi: 10.1134/S1990793124010159
23. Javan MB. Electronic and magnetic properties of monolayer SiC sheet doped with 3d-transition metals. Journal of Magnetism and Magnetic Materials. 2016; 401: 656-661. doi: 10.1016/j.jmmm.2015.10.103
24. Li M, Liu Z, Wu D, et al. Transition Metal-Mediated Preparation of Nitrogen-Doped Porous Carbon for Advanced Zinc-Ion Hybrid Capacitors. Nanomaterials. 2025; 15: 83. doi: 10.3390/nano15020083
25. Wu Y, Zhou LP, Du XZ, Yang Y. Near-field radiative heat transfer between two SiC plates with/without coated metal films. Journal of Nanoscience and Nanotechnology. 2015; 15(4): 3017-3024. doi: 10.1166/jnn.2015.9687
26. Nazeer W, Farooq A, Younas M, et al. On Molecular Descriptors of Carbon Nanocones. Biomolecules. 2018; 8(3): 92. doi: 10.3390/biom8030092
27. Zhao J, Li Z, Cole MT, et al. Nanocone-Shaped Carbon Nanotubes Field-Emitter Array Fabricated by Laser Ablation. Nanomaterials. 2021; 11(12): 3244. doi: 10.3390/nano11123244
28. Rong Y, Cao Y, Guo N, et al. A simple method to synthesize V_2O_5 nanostructures with controllable morphology for high performance Li-ion batteries. Electrochimica Acta. 2016; 222: 1691-1699. doi: 10.1016/j.electacta.2016.11.160
29. Zhu S, Jia H, Wang X, et al. Improved MRD 4H-SiC MESFET with High Power Added Efficiency. Micromachines. 2019; 10: 479. doi: 10.3390/mi10070479
30. Taha HO, El Mahdy AM, El Shemy FES, Hassan MM. Hydrogen storage in SiC, GeC, and SnC nanocones functionalized with nickel, Density Functional Theory—Study. International Journal of quantum Chemistry. 2023; 123(3): e27023. doi: 10.1002/qua.27023
31. Wei T, Zhou Y, Sun C. et al. An intermittent lithium deposition model based on CuMn-bimetallic MOF derivatives for composite lithium anode with ultrahigh areal capacity and current densities. Nano Research. 2023; 17: 2763-2769. doi: 10.1007/s12274-023-6187-8

32. Thupsuri S, Tabtimsai C, Ruangpornvisuti V, Wanno B. A study of the transition metal doped boron nitride nanosheets as promising candidates for hydrogen and formaldehyde adsorptions. Physica E: Low-dimensional Systems and Nanostructures. 2021; 134: 114859. doi: 10.1016/j.physe.2021.114859
33. Mollaamin F, Monajjemi M. Nanomaterials for Sustainable Energy in Hydrogen-Fuel Cell: Functionalization and Characterization of Carbon Nano-Semiconductors with Silicon, Germanium, Tin or Lead through Density Functional Theory Study. Russian Journal of Physical Chemistry B. 2024; 18: 607-623. doi: 10.1134/S1990793124020271
34. Monajjemi M, Mollaamin F. Development of Solid-State Lithium-Ion Batteries (LIBs) to Increase Ionic Conductivity through Interactions between Solid Electrolytes and Anode and Cathode Electrodes. Energies. 2024; 17(18): 4530. doi: 10.3390/en17184530
35. Mollaamin F. Competitive Intracellular Hydrogen-nanocarrier Among Aluminum, Carbon, or Silicon Implantation: a Novel Technology of Eco-Friendly Energy Storage using Research Density Functional Theory. Russian Journal of Physical Chemistry B. 2024; 18: 805-820. doi: 10.1134/S1990793124700131
36. Bo Z, Guo X, Wei X, et al. Density functional theory calculations of NO_2 and H_2S adsorption on the group 10 transition metal (Ni, Pd and Pt) decorated graphene. Physica E: Low-dimensional Systems and Nanostructures. 2019; 109: 156-163. doi: 10.1016/j.physe.2019.01.012
37. Yi Y, Chen J, Zhao Y, et al. Large dielectric properties of niobate-titanate glass ceramics prepared by powder sintering method. Physica B: Condensed Matter. 2024; 694: 416462. doi: 10.1016/j.physb.2024.416462
38. Li S, Tong L, Zhang B, Fu X. First-Principles Study of High-Entropy Sulfides and their Alkali Metal-Doped Modification as Cathode Material for Sodium-Ion Batteries. ChmePhysChem. 2024; 25(17): e202300999. doi: 10.1002/cphc.202300999
39. Guo X, Qin B, Guo Z, et al. Research on desalination performance of novel free-interface evaporation synergism membrane distillation module: Suitable for solar drive scenarios. Separation and Purification Technology. 2025; 361: 131350. doi: 10.1016/j.seppur.2024.131350
40. Jayanthi S, Vahini M, Karthickprabhu S, et al. The Transformative Role of Nano-SiO_2 in Polymer Electrolytes for Enhanced Energy Storage Solutions. Processes. 2024; 12:2174. doi: 10.3390/pr12102174
41. Zolotarev KV, Mikhailov AN, Nakhod VI, et al. Characterization and in vivo toxicity assay of uncoated silicon nanoparticles. New Materials, Compounds and Applications. 2024; 8(2): 162-170. doi: 10.62476/nmca82162
42. Abdullayeva LK, Hasanov MH. Investigation of the role of metal in non-alloy metal-semiconductor (Si) contact. New Materials, Compounds and Applications. 2024; 8(1): 135-141. doi: 10.62476/nmca8135
43. Yanai T, Tew DP, Handy NC. A new hybrid exchange-correlation functional using the Coulomb-attenuating method (CAM-B3LYP), Chemical Physics Letters. 2004; 393(1-3): 51-57. doi: 10.1016/j.cplett.2004.06.011
44. Grimme S, Antony J, Ehrlich S, Krieg H. A consistent and accurate ab initio parametrization of density functional dispersion correction (DFT-D) for the 94 elements H-Pu. The Journal of Chemical Physics. 2010; 132(15): 154104. doi: 10.1063/1.3382344
45. Grimme S, Ehrlich S, Goerigk L. Effect of the damping function in dispersion corrected density functional theory. Journal of Computational Chemistry. 2011; 32(7): 1456-1465. doi: 10.1002/jcc.21759
46. Henkelman G, Arnaldsson A, Jónsson H. A fast and robust algorithm for Bader decomposition of charge density. Computational Materials Science. 2006; 36(3): 354-360. doi: 10.1016/j.commatsci.2005.04.010
47. Ritopečki MS, Skorodumova NV, Dobrota AS, Pašti IA. Density Functional Theory Analysis of the Impact of Boron Concentration and Surface Oxidation in Boron-Doped Graphene for Sodium and Aluminum Storage. C-Journal of Carbon Research. 2023; 9(4): 92. doi: 10.3390/c9040092
48. Mollaamin F, Monajjemi M. Molecular modelling framework of metal-organic clusters for conserving surfaces: Langmuir sorption through the TD-DFT/ONIOM approach. Molecular Simulation. 2023; 49(4): 365-376. doi: 10.1080/08927022.2022.2159996
49. Vosko SH, Wilk L, Nusair M. Accurate spin-dependent electron liquid correlation energies for local spin density calculations: A critical analysis. Canadian Journal of Physics. 1980; 58(8): 1200-1211. doi: 10.1139/p80-159
50. Frisch MJ, Trucks GW, Schlegel HB, et al. Gaussian 16, Revision C.01. Available online: https://gaussian.com/ (accessed on 10 January 2025).
51. Dennington R, Keith TA, Millam JM. GaussView, Version 6.06.16. Available online: https://gaussian.com/gv6new/ (accessed on 10 January 2025).

52. Trontelj Z, Pirnat J, Jazbinšek V, et al. Nuclear Quadrupole Resonance (NQR)—A Useful Spectroscopic Tool in Pharmacy for the Study of Polymorphism. Crystals. 2020; 10(6): 450. doi: 10.3390/cryst10060450
53. Sciotto R, Ruiz Alvarado IA, Schmidt WG. Substrate Doping and Defect Influence on P-Rich InP (001): H Surface Properties. Surfaces. 2024; 7(1): 79-87. doi: 10.3390/surfaces7010006
54. Luo J, Wang C, Wang Z, et al. NMR and NQR studies on transition-metal arsenide superconductors $LaRu_2As_2$, $KCa_2Fe_4As_4F_2$, and $A_2Cr_3As_3$. Chinese Physics B. 2020; 29: 067402. doi: 10.1088/1674-1056/ab892d
55. Young HD, Freedman RA, Ford AL. Sears and Zemansky's University Physics with Modern Physics, 13th ed. Addison-Wesley; 2012. p. 754.
56. Sohail U, Ullah F, Binti Zainal Arfan NH, et al. Transition Metal Sensing with Nitrogenated Holey Graphene: A First-Principles Investigation. Molecules. 2023; 28: 4060. doi: 10.3390/molecules28104060.
57. Sheet SHM, Mahmod RB, Saeed NHM, Saied SM. Theoretical study for comparison of pKa of a number of Schiff bases by employing parameters derived from DFT and MP2 method. New Materials, Compounds and Applications. 2024; 8(1): 94-108. doi: 10.62476/nmca8194